Structural Chemistry
https://doi.org/10.1007/s11224-022-02079-8

ORIGINAL RESEARCH

In silico analyses of betulin: DFT studies, corrosion inhibition properties, ADMET prediction, and molecular docking with a series of SARS-CoV-2 and monkeypox proteins

Tatyana M. Burkhanova[1,2] · Alena I. Krysantieva[1] · Maria G. Babashkina[1] · Irina A. Konyaeva[1] · Lyudmila N. Monina[1] · Anastasiya N. Goncharenko[1] · Damir A. Safin[1,2]

Received: 19 June 2022 / Accepted: 6 October 2022
© The Author(s), under exclusive licence to Springer Science+Business Media, LLC, part of Springer Nature 2022

Abstract
We report detailed computational studies of betulin — a pentacyclic naturally occuring triterpene, which is a precursor for a broad family of biologically active derivatives. The structure, electronic, and optical properties of betulin were studied by the density functional theory (DFT) calculations in gas phase. The reactivity and the reactive centers of betulin were revealed through its global reactivity descriptors and molecular electrostatic potential (MEP). The DFT calculations were also applied to probe betulin as a potential corrosion inhibitor for some important metals used in implants. Electron charge transfer from the molecule of betulin to the surface of all the examined metals (Ti, Fe, Zr, Co, Cu, Cr, Ni, Mn, Mo, Zn, Al, W, Ag, Au) was revealed, of which the best results were obtained for Ni, Au and Co. Bioavailability, druggability as well as absorption, distribution, metabolism, excretion and toxicity (ADMET) properties of betulin were evaluated using the SwissADME, BOILED-Egg and ProTox-II tools. Molecular docking was applied to examine the influence of the title compound on a series of the SARS-CoV-2 proteins as well as one of the monkeypox proteins. It was established that betulin is active against all the applied proteins with the best binding affinity with papain-like protease (PLpro) and spike protein (native) of SARS-CoV-2. The title compound is also active against the studied monkeypox protein. Interaction of betulin with papain-like protease (PLpro) was studied using molecular dynamics simulations.

Keywords Betulin · Computational study · DFT · ADMET · Corrosion inhibitor · Molecular docking

Introduction

Nature seems to be the most efficient designer and producer of biologically active substances that are of great importance and value for the fabrication of drugs. Throughout the whole history of the mankind, nature has become a bottomless pantry of drugs or their components, which are used for the treatment or in therapy of different diseases. Just sufficient to say, nature was the only source of, e.g., quinine, strychnine, morphine, aspirin, penicillin and many other bioactive compounds called natural products. The latter three products are also known as key milestones in the development of commercial production of medicines. Even today, natural compounds have not lost their relevance, but on the contrary, they are attracting more and more attention due to both their unique properties and commercial perspectives [1].

Of a myriad of natural products, terpenes are a large class comprising several tens of thousands of compounds. According to the IUPAC Gold Book, terpenes are *hydrocarbons of biological origin having carbon skeletons formally derived from isoprene. This class is subdivided into the* C_5 *hemiterpenes*, C_{10} *monoterpenes*, C_{15} *sesquiterpenes*, C_{20} *diterpenes*, C_{25} *sesterterpenes*, C_{30} *triterpenes*, C_{40} *tetraterpenes (carotenoids) and* C_{5n} *polyterpenes* [2, 3]. These hydrocarbons are obtained primarily from plants [4] and are of particular interest for both industrial application and medicine. Nowadays, of the triterpene subclass representatives, betulin

✉ Damir A. Safin
damir.a.safin@gmail.com

[1] Advanced Materials for Industry and Biomedicine Laboratory, Kurgan State University, Sovetskaya Str. 63/4, Kurgan 640020, Russian Federation

[2] Scientific and Educational and Innovation Center for Chemical and Pharmaceutical Technologies, Ural Federal University Named After the First President of Russia B.N. Yeltsin, Mira Str. 19, Ekaterinburg 620002, Russian Federation

Published online: 27 October 2022

(3-lup-20(29)-ene-3β,28-diol) seems to be one of the most attractive compounds, especially for its pharmacological and anticancer properties, and as a precursor of new drugs [5–7]. Betulin, which is also known as betuline, betulinol or betulinic alcohol, is a pentacyclic lupane-type triterpene (Fig. 1). It was one of the first natural products obtained by Lowitz in 1788 [8], which structure was elucidated in 1952. The main natural source of betulin nowadays is the birch bark, from which the title compound can efficiently be extracted [9, 10]. The content of betulin in the birch bark can vary from about 10% up to about 35% depending on a number of different factors such as the type of birch, the age of the tree, growth conditions and place [9, 10]. Considering betulin as a chemical reagent, it has three functionalities, namely two hydroxyl groups and isopropenyl fragment (Fig. 1), which can be involved in chemical modifications, yielding a rich panel of derivatives with a wide spectrum of properties of value. Thus, betulin is an important and valuable precursor.

On the other hand, corrosion of metals and metallic materials is one of the main problems of industry, including medical industry especially where metal-based biomedical implants are used [11–13]. As one of the most efficient corrosion inhibitors, organic compounds have been of particular interest and quantum chemical calculations have become a powerful tool to probe molecule-surface bonding, that is crucial for corrosion inhibition [14–18].

With all this in mind, as well as in continuation of our ongoing interest in in silico studies of bioactive compounds [19–29], we have directed our attention to betulin. Theoretical calculations based on density functional theory (DFT) were performed to examine electronic properties of this compound. The global chemical reactivity descriptors were estimated from the energy of the HOMO and LUMO orbitals to examine the relative reactivity of the molecule. We have also applied the DFT calculations to probe betulin as a potential corrosion inhibitor for some important metals used in implants. ADMET properties of betulin were additionally evaluated. Molecular docking and molecular dynamics simulations were applied to probe interaction of betulin with a series of the SARS-CoV-2 proteins as well as one of the monkeypox proteins.

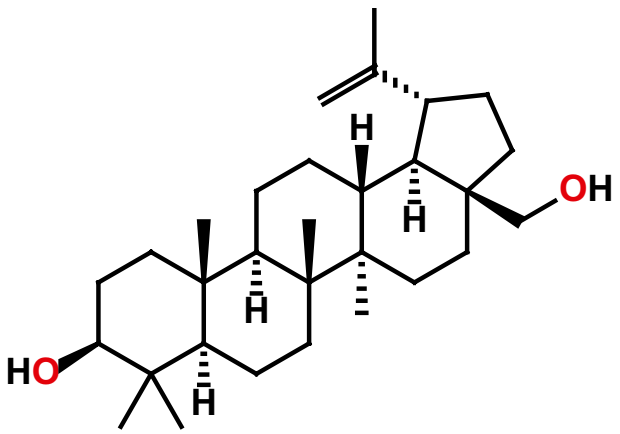

Fig. 1 Diagram of betulin

Experimental

Computational details

The ground state geometry of betulin in gas phase was fully optimized without symmetry restrictions. The calculations were performed by means of the GaussView 6.0 molecular visualization program [30] and the Gaussian 09, Revision D.01 program package [31], using the DFT method with Becke-three-parameter-Lee–Yang–Parr (B3LYP) hybrid functional [32, 33] and 6-311G++(d,p) [32, 34] basis set. The electronic isosurfaces of the molecular orbitals and molecular electrostatic potential (MEP) surface were generated from the fully optimized ground state geometry obtained by using the B3LYP/6–311++G(d,p) method. The density-of-states (DOS) plot was calculated using the GaussSum 3.0 software [35, 36].

In silico drug-likeness analysis

Bioavailability, druggability and toxicity properties of betulin were evaluated using the SwissADME [37], BOILED-Egg [38] and ProTox-II [39, 40] tools.

Molecular docking

Molecular docking simulations of the optimized structure of betulin with a series of the SARS-CoV-2 proteins and A42R profilin-like protein from monkeypox virus Zaire-96-I-16 were carried out with AutoDock Vina [41, 42], using the Lamarckian genetic algorithm (LGA) scoring function with number of GA runs = 100, population size = 500 and maximum number of evaluations = 25 000 000. The targeted protein structures were acquired via the RCSB PDB database [43] and were pretreated before the docking, including water removing, and inserting hydrogen atoms and missing residues and charges. Gasteiger charges were added to the ligand molecules prior converting to PDBQT format. AutoDock Tools (v. 1.5.7) was utilized to define the grid box with the dimensions of 30 × 30 × 30 Å with 0.375 Å grid spacing. Semi flexible docking was performed keeping the receptor molecule rigid and ligands flexible. During the docking procedure, 200 conformations for each ligand were left flexible, while the protein was held rigid. The lowest binding energy conformers and 2D interactions were filtered

from 10 top-ranked poses. BIOVIA Discovery Studio 2020 [44] was utilized for visualization of the docked conformations and 3D target-ligand interactions.

Molecular dynamics simulation

Molecular dynamics (MD) simulations of the complex of betulin with papain-like protease (PLpro) were performed using the WebGRO on-line service [45]. Parameters such as root mean square deviation (RMSD), root mean square fluctuation (RMSF), radius of gyration (Rg), solvent accessible surface area (SASA) and intermolecular hydrogen bonds were assessed. The complex was prepared for MD using GROMOS96 43a1 forcefield and was equilibrated using the canonical (NVT) and the isothermal–isobaric (NPT) ensembles. The betulin topology was generated with the PRODRG tool [46]. Simple point charge (SPC) was used as a solvent model (triclinic water box with size $50 \times 75 \times 70$ Å) for protein–betulin complex [47]. This system was neutralized by adding sodium or chlorine ions based on the total charges. For minimization of the system before MD, the steepest descent algorithm (5000 steps) was applied. The MD simulations were performed in the presence 0.15 M NaCl using the constant temperature (310 K) and pressure (1.0 bar). Approximate number of frame per simulation was 1000. The simulation time was set to 100 ns.

Results and discussion

We have applied the DFT calculations to probe the electronic properties of betulin. Firtsly, the structure of betulin was optimized in gas phase at 298.15 K, using the DFT/B3LYP/6–311++G(d,p) method. In the optimized structure, all the cyclohexane cycles adopt a chair conformation, while the cyclopentane fragment adopts an envelope conformation (Fig. 2). The obtained bond lengths and angles are typical. Particularly, the C–C bond lengths vary from 1.510 to 1.612 Å (Table 1), indicating their single bond nature. Interestingly, the longest C–C bond length was revealed for the C39–C82 bond (Table 1), which is formed between the two opposite quaternary carbon atoms of the central cyclohexane ring, thus possessing a certain degree of repulsion due to steric hindrance (Fig. 2). The C71–C79 bond length is 1.335 Å, characteristic for a double bond. Finally, the two C–O bonds are 1.432 and 1.434 Å (Table 1). The C–C–C bond angles, formed by two single bonds, vary from 100.80 to 120.15° (Table 1), with the lowest values corresponding to the cyclopentane intracyclic bond angles (Fig. 2 and Table 1). The sum of the C–C–C bond angles around the C71 carbon atom is almost 360° (359.91°), indicating its sp^2-hybridization. In general, the geometrical parameters of the optimized molecule of betulin are in excellent agreement with those found in a number of solvate structures collected in the Cambridge Structural Database (CSD) [48].

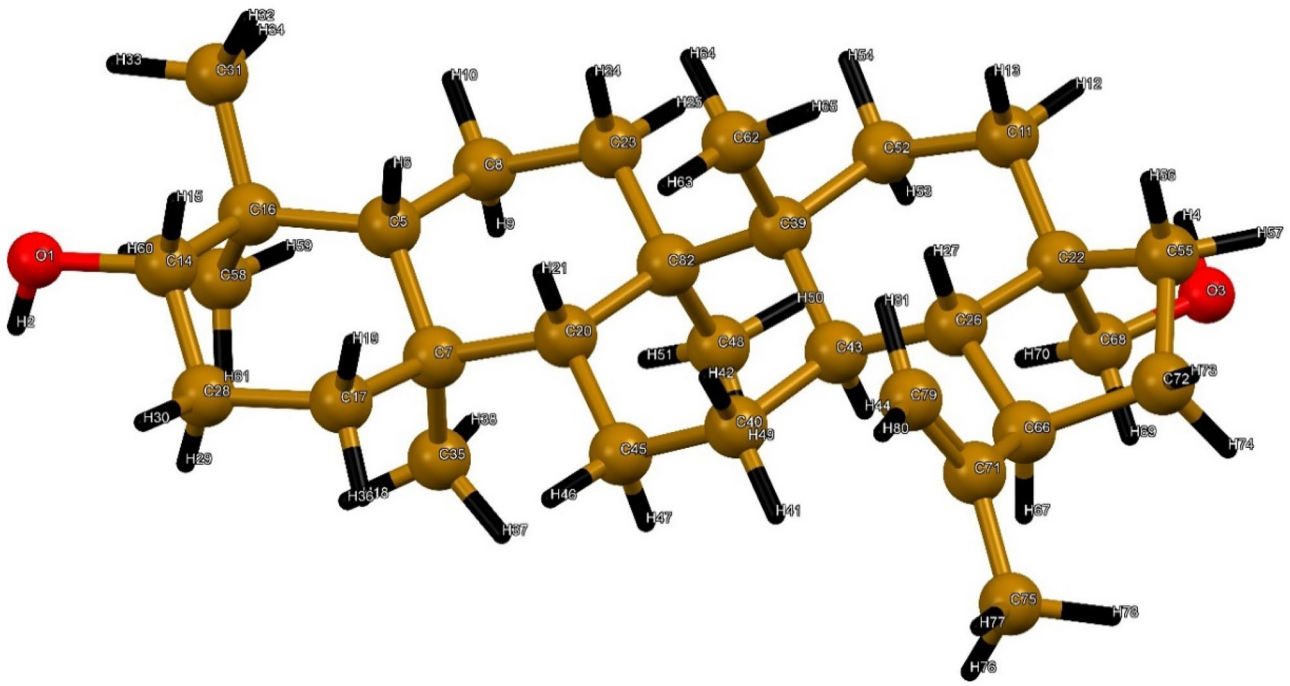

Fig. 2 The optimized structure of betulin, obtained using the DFT/B3LYP/6-311G++(d,p) method

Table 1 Selected bond lengths (Å) and bond angles (°) in the optimized structure of betulin, obtained using the DFT/B3LYP/6-311G++(d,p) method (see Fig. 2 for atoms labeling)

Bond length					
C5–C7	1.569	C16–C58	1.543	C39–C62	1.553
C5–C8	1.536	C17–C28	1.533	C39–C82	1.612
C5–C16	1.570	C20–C45	1.543	C40–C43	1.536
C7–C17	1.554	C20–C82	1.575	C40–C45	1.537
C7–C20	1.584	C22–C26	1.556	C48–C82	1.551
C7–C35	1.549	C22–C55	1.539	C55–C72	1.549
C8–C23	1.534	C22–C68	1.552	C66–C71	1.521
C11–C22	1.535	C23–C82	1.551	C66–C72	1.580
C11–C52	1.545	C26–C43	1.541	C71–C75	1.510
C14–C16	1.557	C26–C66	1.549	C71–C79	1.335
C14–C28	1.525	C39–C43	1.577	C14–O1	1.434
C16–C31	1.546	C39–C52	1.562	C68–O3	1.432
Bond angle					
C5–C7–C17	107.42	C16–C14–C28	113.50	C39–C43–C40	111.06
C5–C7–C20	106.55	C17–C7–C20	107.84	C39–C82–C48	110.56
C5–C7–C35	114.21	C17–C7–C35	107.74	C43–C26–C66	120.15
C5–C8–C23	110.97	C20–C7–C35	112.80	C43–C39–C52	110.23
C5–C16–C14	107.34	C20–C45–C40	113.08	C43–C39–C62	109.96
C5–C16–C31	109.31	C20–C82–C23	109.48	C43–C39–C82	108.16
C5–C16–C58	114.43	C20–C82–C39	107.87	C43–C40–C45	112.52
C7–C5–C8	110.73	C20–C82–C48	111.51	C45–C20–C82	110.69
C7–C5–C16	117.58	C22–C11–C52	111.93	C52–C39–C62	105.80
C7–C17–C28	113.81	C22–C26–C43	112.16	C52–C39–C82	111.16
C7–C20–C45	114.06	C22–C26–C66	104.54	C55–C22–C68	108.40
C7–C20–C82	117.07	C22–C55–C72	104.13	C55–C72–C66	106.31
C8–C5–C16	114.36	C23–C82–C39	110.76	C62–C39–C82	111.53
C8–C23–C82	114.33	C23–C82–C48	106.68	C66–C71–C75	114.24
C11–C22–C26	107.87	C26–C22–C55	100.80	C66–C71–C79	124.70
C11–C22–C55	116.27	C26–C22–C68	112.78	C71–C66–C72	110.60
C11–C22–C68	110.47	C26–C43–C39	110.87	C75–C71–C79	120.97
C11–C52–C39	115.21	C26–C43–C40	114.83	O1–C14–C16	112.79
C14–C16–C31	106.88	C26–C66–C71	118.21	O1–C14–C28	111.08
C14–C16–C58	111.26	C26–C66–C72	103.78	O3–C68–C22	113.08
C14–C28–C17	112.26	C31–C16–C58	107.36		

Analysis of the Mulliken atomic charges in the optimized structure of betulin revealed that all the hydrogen atoms are positively charged varying from 0.072 to 0.243 a.u. with the highest values corresponding to the hydroxyl hydrogen atoms (Fig. 3). Of non-hydrogen atoms, exclusively the C22, C26, and C71 carbon atoms carry the positive charge ranging from 0.074 to 0.115 a.u., while the C14 and C55 carbons are the most negatively charged and of −0.647 and −0.548 a.u., respectively (Fig. 3). Finally, the oxygen atoms are both negatively charged and of −0.152 and −0.198 a.u. (Fig. 3).

The electrophilic and nucleophilic sites in a molecule of betulin were revealed using the molecular electrostatic potential (MEP) analysis. On the MEP surface of betulin, the most pronounced nucleophilic (red color) and electrophilic (blue color) centers are located, as expected, on the hydroxyl oxygen and hydrogen atoms, respectively (Fig. 4).

According to the DFT calculations, the dipole moment of betulin in gas phase is 0.7627 Debye with the highest contribution of the μ_z component (Table 2). Such low dipole moment is due to the overall balance in the charge from one side of a molecule to the other side as evidenced from the corrsponding MEP surface (Fig. 4). The energies of the highest occupied molecular orbital (HOMO) and lowest lying unoccupied molecular orbital (LUMO) for betulin are −6.71768 and −0.46069 eV, respectively, with the energy gap of 6.25699 eV (Table 2). The HOMO is mainly delocalized over the isopropenylcyclopentane fragment,

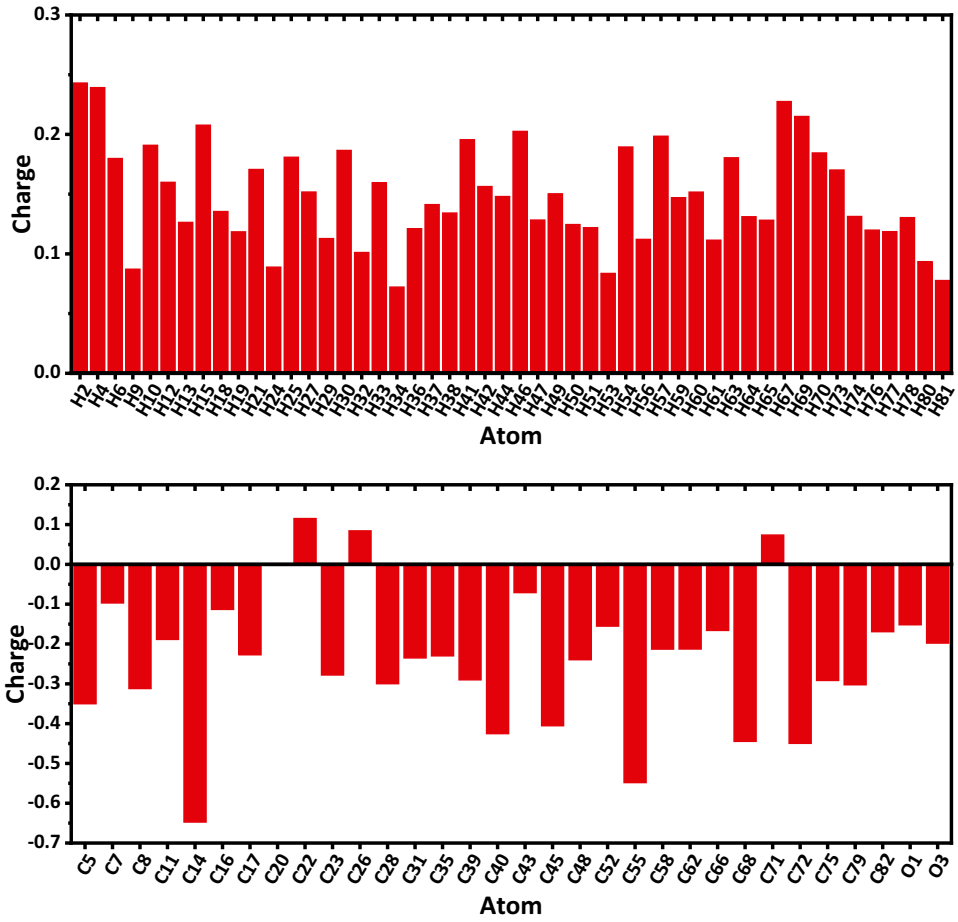

Fig. 3 Mulliken atomic charges in the optimized structure of betulin, obtained using the DFT/B3LYP/6-311G++(d,p) method (see Fig. 2 for atoms labeling)

while the LUMO is mainly spread around the CH_2OH fragment (Fig. 5). The density-of-states (DOS) plot of betulin is shown in Fig. 6. Chemical potential (μ) was found to be −3.58919 eV, indicating electron donating ability and low electron accepting ability. The chemical hardness (η) describes the resistance towards deformation/polarization of the electron cloud of the molecule upon a chemical reaction, while softness (S) is a reverse of chemical hardness. The title compound is characterized by a relatively high value of the chemical hardness and a relatively low value of the chemical softness, indicating it exhibits a strong tendency to exchange its electron cloud with surrounding environment (Table 2). The electrophilicity index (ω), which is denoted as the energy of stabilization to accept electrons, is 2.05886 eV. This value is characteristic for strong electrophiles [49]. Finally, a molecule of betulin can accept about 1.15 electrons as evidenced from the ΔN_{max} value (Table 2).

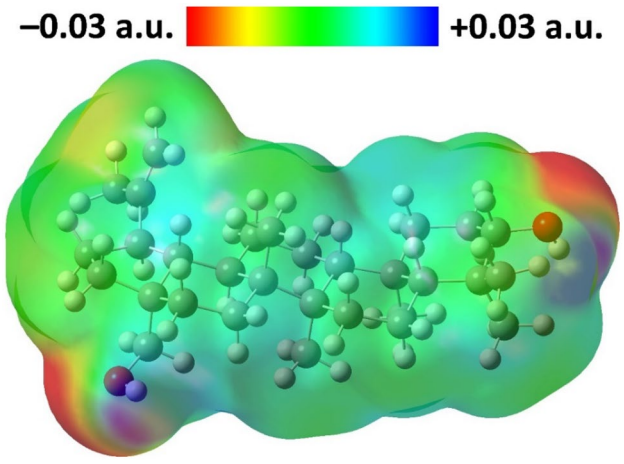

Fig. 4 View of the molecular electrostatic potential surface of betulin, obtained using the DFT/B3LYP/6-311G++(d,p) method

The HOMO and LUMO values are of importance to estimate corrosion inhibition properties of a compound [14–17]. This becomes even more crucial considering metal-based biomedical implants [11–13]. We have also probed potential corrosion inhibition properties of betulin toward a series of metals, which are prominent components of biomedical implants (Table 2) [13]. As such, we have used the most reliable equation, which includes the so-called work function (Φ) [50], to calculate electron charge transfer (Table 2) [18]. According to the obtained results, it was revealed electron charge transfer from the

Table 2 Dipole moment, frontier molecular orbitals, gap value, descriptors, and molecule-to-metal electron charge transfer values for betulin in gas phase, obtained using the DFT/B3LYP/6–311++G(d,p) method

μ_x (Debye)	−0.1182
μ_y (Debye)	−0.0317
μ_z (Debye)	0.7529
μ_D (Debye)	0.7627
E_{HOMO} (eV)	−6.71768
E_{LUMO} (eV)	−0.46069
$\Delta E_{LUMO-HOMO} = E_{LUMO} - E_{HOMO}$ (eV)	6.25699
Ionization energy, $I = -E_{HOMO}$ (eV)	6.71768
Electron affinity, $A = -E_{LUMO}$ (eV)	0.46069
Electronegativity, $\chi = (I+A)/2$ (eV)	3.58919
Chemical potential, $\mu = -\chi$ (eV)	−3.58919
Global chemical hardness, $\eta = (I - A)/2$ (eV)	3.12850
Global chemical softness, $S = 1/(2\eta)$ (eV^{-1})	0.15982
Global electrophilicity index, $\omega = \mu^2/(2\eta)$ (eV)	2.05886
Maximum additional electric charge, $\Delta N_{max} = -\mu/\eta$	1.14726
Molecule-to-metal electron charge transfer, $\Delta N_{betulin} = (\Phi - \chi)/\eta$:	
Ti	0.24
Fe	0.29
Zr	0.15
Co	0.45
Cu	0.34
Cr	0.29
Ni	0.50
Mn	0.16
Mo	0.32
Zn	0.24
Al	0.22
W	0.31
Ag	0.21
Au	0.48
Total negative charge, TNC (e)	−7.70926

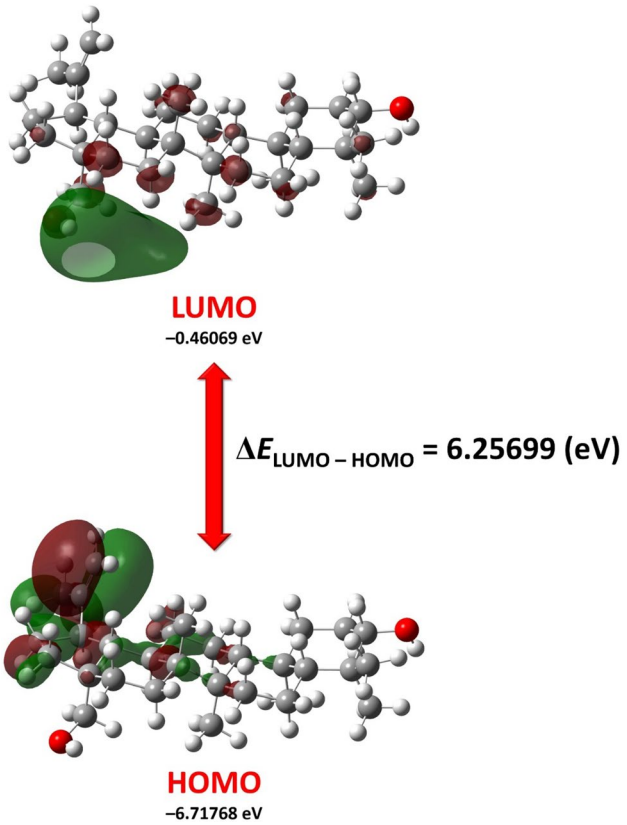

Fig. 5 Energy levels and views on the electronic isosurfaces of the HOMO and LUMO of the ground state of betulin, obtained using the DFT/B3LYP/6-311G++(d,p) method

molecule of betulin to the surface of all the studied metals, of which the most efficient electron charge transfer was established for Ni, Au and Co (Table 2). Total negative charge (TNC) value is a parameter to indicate an adsorption of a molecule-inhibitor onto a metal surface and defined as a sum of negative Mulliken charges of atoms. As higher the absolute value of TNC as better a molecule will donate electrons to the metal surface, thus exhibiting better corrosion inhibition efficiency. For betulin, the TNC value was calculated as −7.70926 electrons (Table 2).

Interestingly, corrosion inhibition properties toward some of the metals estimated for betulin are comparable (and even superior) with those recently obtained for different tautomers of salen [29]. Notably, the latter compound belongs to salicylaldehyde based Schiff bases — a prominent class of corrosion inhibitors [51–53].

According to ProTox-II, a virtual lab for the prediction of toxicities of small molecules [39, 40], betulin belongs to the fourth class of toxicity (Fig. 7). As evidenced from the SwissADME [37] bioavailability radar, the title compound is highly preferred in four parameters, namely size, polarity, insaturation and flexibility, while it has a relatively poor result in the lipophilicity and insolubility parameters (Fig. 7). The latter features are obviously due to an extended polycyclic hydrocarbon structure of betulin. It was predicted that betulin is likely a pronounced inhibitor of enzyme, cytochrome P450, and nuclear receptor with the probabilities of 33.3%, 20.0% and 13.3%, respectively (Fig. 7). According to the toxicity model report, betulin was revealed to be inactive toward the listed targets (Fig. 7).

The BOILED-Egg method was found to be efficient to predict the human blood–brain barrier (BBB) penetration and gastrointestinal absorption [38]. This approach is based on lipophilicity (WLOGP) and polarity (topological polar surface area, TPSA) (Fig. 7). Points located in the yellow region (BOILED-Egg's yolk) are molecules

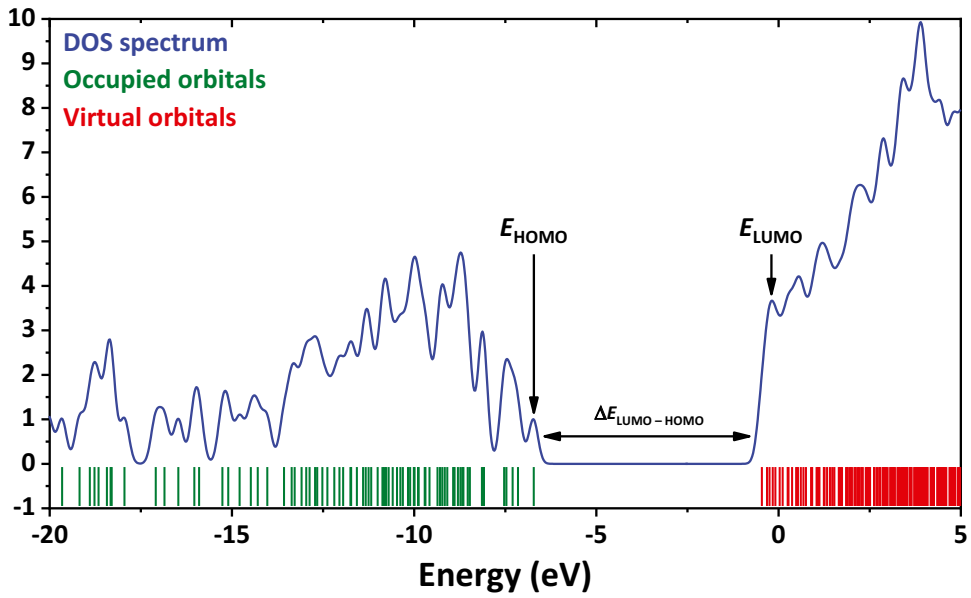

Fig. 6 The DOS plot for betulin, obtained using the DFT/B3LYP/6-311G++(d,p) method

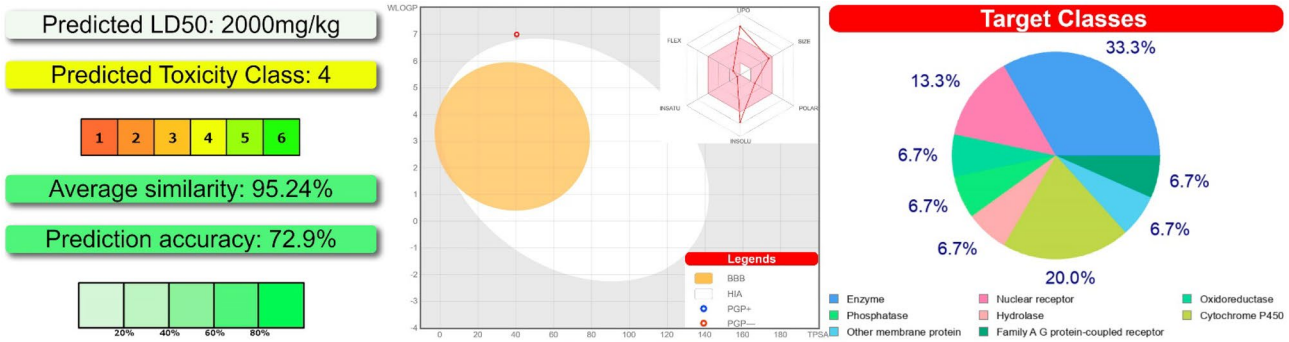

Toxicity Model Report

Classification	Target	Shorthand	Prediction	Probability
Organ toxicity	Hepatotoxicity	dili	Inactive	0.88
Toxicity end points	Carcinogenicity	carcino	Inactive	0.65
Toxicity end points	Immunotoxicity	immuno	Inactive	0.50
Toxicity end points	Mutagenicity	mutagen	Inactive	0.79
Toxicity end points	Cytotoxicity	cyto	Inactive	0.98
Tox21-Nuclear receptor signalling pathways	Aryl hydrocarbon Receptor (AhR)	nr_ahr	Inactive	0.98
Tox21-Nuclear receptor signalling pathways	Androgen Receptor (AR)	nr_ar	Inactive	0.94
Tox21-Nuclear receptor signalling pathways	Androgen Receptor Ligand Binding Domain (AR-LBD)	nr_ar_lbd	Inactive	0.91
Tox21-Nuclear receptor signalling pathways	Aromatase	nr_aromatase	Inactive	0.96
Tox21-Nuclear receptor signalling pathways	Estrogen Receptor Alpha (ER)	nr_er	Inactive	0.80
Tox21-Nuclear receptor signalling pathways	Estrogen Receptor Ligand Binding Domain (ER-LBD)	nr_er_lbd	Inactive	0.96
Tox21-Nuclear receptor signalling pathways	Peroxisome Proliferator Activated Receptor Gamma (PPAR-Gamma)	nr_ppar_gamma	Inactive	0.99
Tox21-Stress response pathways	Nuclear factor (erythroid-derived 2)-like 2/antioxidant responsive element (nrf2/ARE)	sr_are	Inactive	0.63
Tox21-Stress response pathways	Heat shock factor response element (HSE)	sr_hse	Inactive	0.63
Tox21-Stress response pathways	Mitochondrial Membrane Potential (MMP)	sr_mmp	Inactive	0.57
Tox21-Stress response pathways	Phosphoprotein (Tumor Supressor) p53	sr_p53	Inactive	0.71
Tox21-Stress response pathways	ATPase family AAA domain-containing protein 5 (ATAD5)	sr_atad5	Inactive	0.98

Fig. 7 Toxicity results, calculated by ProTox-II (top-left and bottom), druggability predictions (top-right), BOILED-Egg model (top-middle) together with the bioavailability radar within the domain borders of ADME properties, calculated by SwissADME, of betulin (the colored zone of the radar is the suitable physicochemical space for oral bioavailability)

Table 3 The best poses of betulin inside the binding sites of the listed proteins

Protein	PDB code	Betulin
Main protease (Mpro)	6LU7	−7.3(0)
Papain-like protease (PLpro)	6WUU	**−9.6(0)**
Nonstructural protein 3 (nsp3_range 207–379-AMP)	6W6Y	−7.7(0)
Nonstructural protein 3 (nsp3_range 207–379-MES)	6W6Y	−6.1(1)
RdRp-RNA	7BV2	−7.2(1)
Nonstructural protein 14 (N7-MTase)	5C8S	−7.5(1)
Nonstructural protein 15 (endoribonuclease)	6WLC	−5.3(1)
Nonstructural protein 16 (GTA site)	6WVN	−7.4(0)
Nonstructural protein 16 (MGP site)	6WVN	−6.6(0)
Nonstructural protein 16 (SAM site)	6WVN	−7.6(0)
Spike protein, RBD (native)	6M0J	**−7.8(1)**
Spike protein, RBD (mutated)	6M0J	**−7.0(1)**
A42R profilin-like protein from monkeypox (strain Zaire-96-I-16)	4QWO	**−6.2(1)**

predicted to passively permeate through the BBB, while points located in the white region (BOILED Egg's white) are molecules predicted to be passively absorbed by the gastrointestinal tract. Blue (PGP+) and red (PGP–) dots are for molecules predicted to be effluated and not to be effluated from the central nervous system by the P-glycoprotein, respectively. As evidenced from the red dot position for betulin, both BBB and gastrointestinal absorption properties are negative with the negative PGP effect on the molecule (Fig. 7). This is explained by a high WLOGP value of 7.00 (Fig. 7).

We have further applied a molecular docking approach for betulin against a series of SARS-CoV-2 proteins. This approach allows to visualize and explicate interaction between a small compound as a ligand and biomolecule as a target [54]. This application is one of the most broadly exerted technique to examine the structure–activity relationship and biological activity in the drug discovery [55]. Docking is the best option to diminish the time and cost of synthesis of molecules of interest. In addition, it is considered a current and advantageous method to have insight information of the possible binding site of the ligand in the protein [56].

In this study, molecular docking was employed to rationalize betulin in the SARS-CoV-2 targets. The target structures were primarily selected in accordance with the structural features of the virus [57, 58] as well as based on biological mechanisms and functions that can be utilized to reduce, prevent or treat the virus [59] (Table 3).

According to the docking analysis results, betulin was found to be active against all the applied SARS-CoV-2 proteins with the best binding affinity with papain-like protease (PLpro) and spike protein, RBD (native) (Fig. 8 and Table 3). Complexes of betulin with these proteins are exclusively defined with a conventional hydrogen bond with TYR268 and ASN343, respectively (Fig. 8 and Table 4). However, interaction of betulin with spike protein, RBD (mutated) is less efficient (Table 3), which is explained by the complex formation through a much weaker conventional hydrogen bond with GLY354, although two alkyl interactions with ALA386 and ALA387 are also formed (Fig. 8 and Table 4).

The obtained molecular docking results for betulin are comparable with those found for initial redocked ligands [23], remdesivir [23], molnupiravir [25] and different tautomers of salen [29], and superior to those calculated for favipiravir [23]. Thus, betulin can be considered a promising agent against COVID-19.

Nowadays, besides the COVID-19 pandemic, the other infectious viral disease, namely monkeypox, is continuously rising [60]. With this in mind, we have also probed betulin as a potential inhibitor toward one of the monkeypox proteins, viz. A42R profilin-like protein from monkeypox (strain Zaire-96-I-16). It was found that betulin is also active against the applied monkeypox protein (Table 3) and interacts through a conventional hydrogen bond with THR126 and an alkyl interaction with ARG129 (Fig. 8 and Table 4).

We have also performed molecular dynamics (MD) simulations of 100 ns at 310 K to evaluate interactions in the betulin complex with papain-like protease (PLpro), which showed the most remarkable docking score. Particularly, the complex showed an RMSD below 0.476 nm with the average value of 0.381 nm (Fig. 9). The RMSF value for the same complex of PLpro with betulin was below 0.605 nm with the strongest fluctuations observed for GLU1 and LEU317, followed by VAL11, ASN13, HIS17, SER24, MET25, GLN29, LYS43, LYS45, ASN48, GLU51, GLN97, ASN99, THR191, LYS228, and LYS315 (Fig. 9). Rg values for this complex form a relatively stable profile from 2.457 to 2.603 nm (Fig. 9). The SASA profile was calculated for predicting the interaction between the complex of PLpro with betulin and solvents. It was established that the binding of betulin to PLpro did not impair the protein's interaction with the solvent molecule and the stability of the protein (Fig. 9). During the 100 ns simulation time, the average SASA was calculated as 255.08 nm^2. It was also observed that the complex forms 1 intermolecular hydrogen bond during almost the whole simulation time; 2 intermolecular hydrogen bonds at about 13–40, 50–75, 80–86, 94–97 ns; and 3 intermolecular hydrogen bonds at about 55–70 ns (Fig. 9).

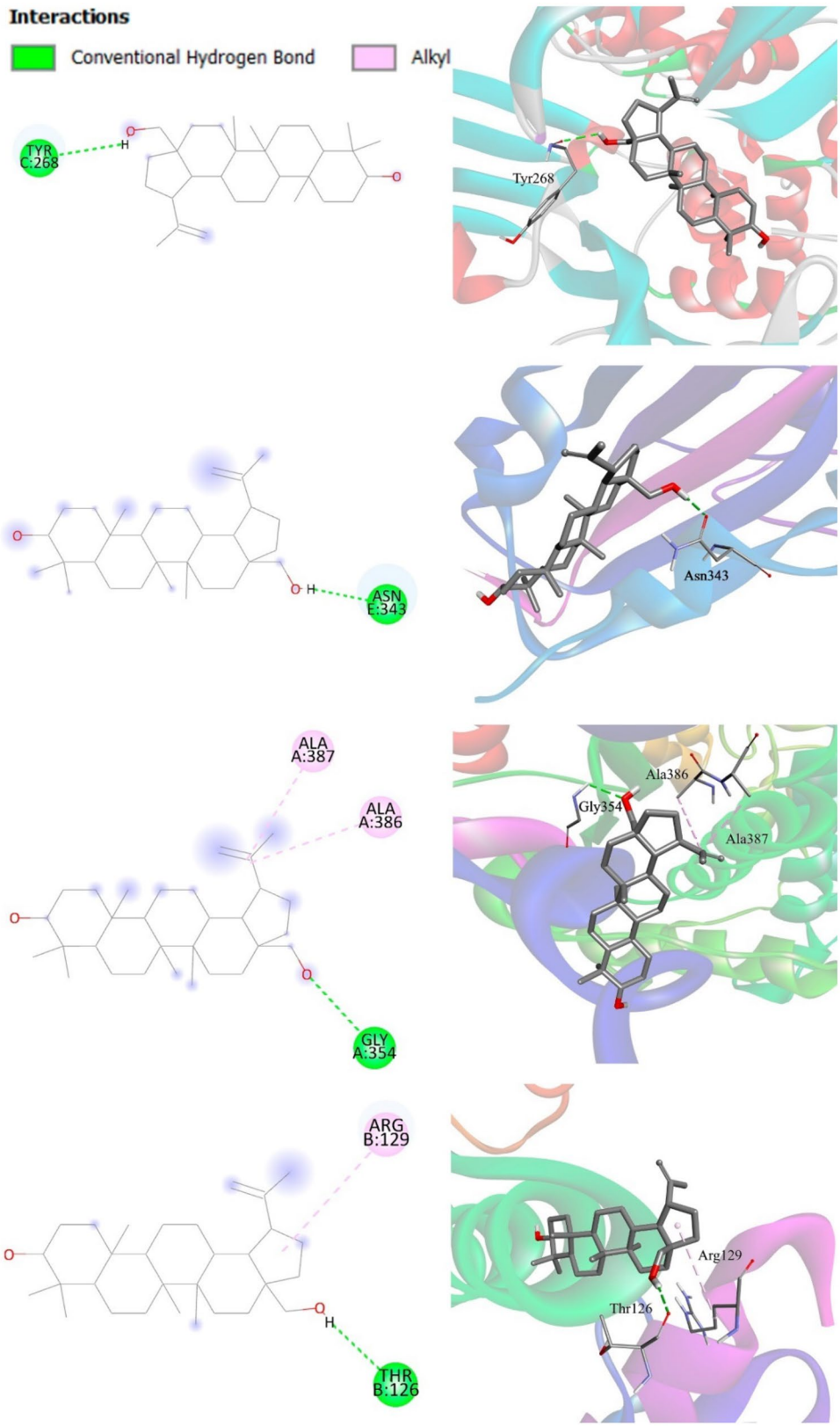

Fig. 8 2D (left) and 3D (right) views on the interaction of betulin with (from top to bottom) papain-like protease (PLpro), spike protein (native), spike protein (mutated) and A42R profilin-like protein from monkeypox (strain Zaire-96-I-16)

Table 4 The best types of interactions and distances of betulin with papain-like protease (PLpro), spike protein (native), spike protein (mutated) and A42R profilin-like protein from monkeypox (strain Zaire-96-I-16)

Interaction	Distance (Å)	Bonding	Bonding type
Papain-like protease (PLpro)–betulin			
:betulin:H-C:TYR268:O	2.57995	Hydrogen bond	Conventional hydrogen bond
Native spike protein, RBD–betulin			
:betulin:H-E:ASN343:OD1	2.00885	Hydrogen bond	Conventional hydrogen bond
Mutated spike protein, RBD–betulin			
A:GLY354:HN-:betulin:O	2.56611	Hydrogen bond	Conventional hydrogen bond
A:ALA386-:betulin	4.65949	Hydrophobic	Alkyl
A:ALA387-:betulin	3.94989	Hydrophobic	Alkyl
A42R profilin-like protein from monkeypox (strain Zaire-96-I-16)–betulin			
:betulin:H-B:THR126:O	2.34173	Hydrogen bond	Conventional hydrogen bond
B:ARG129-:betulin	5.48297	Hydrophobic	Alkyl

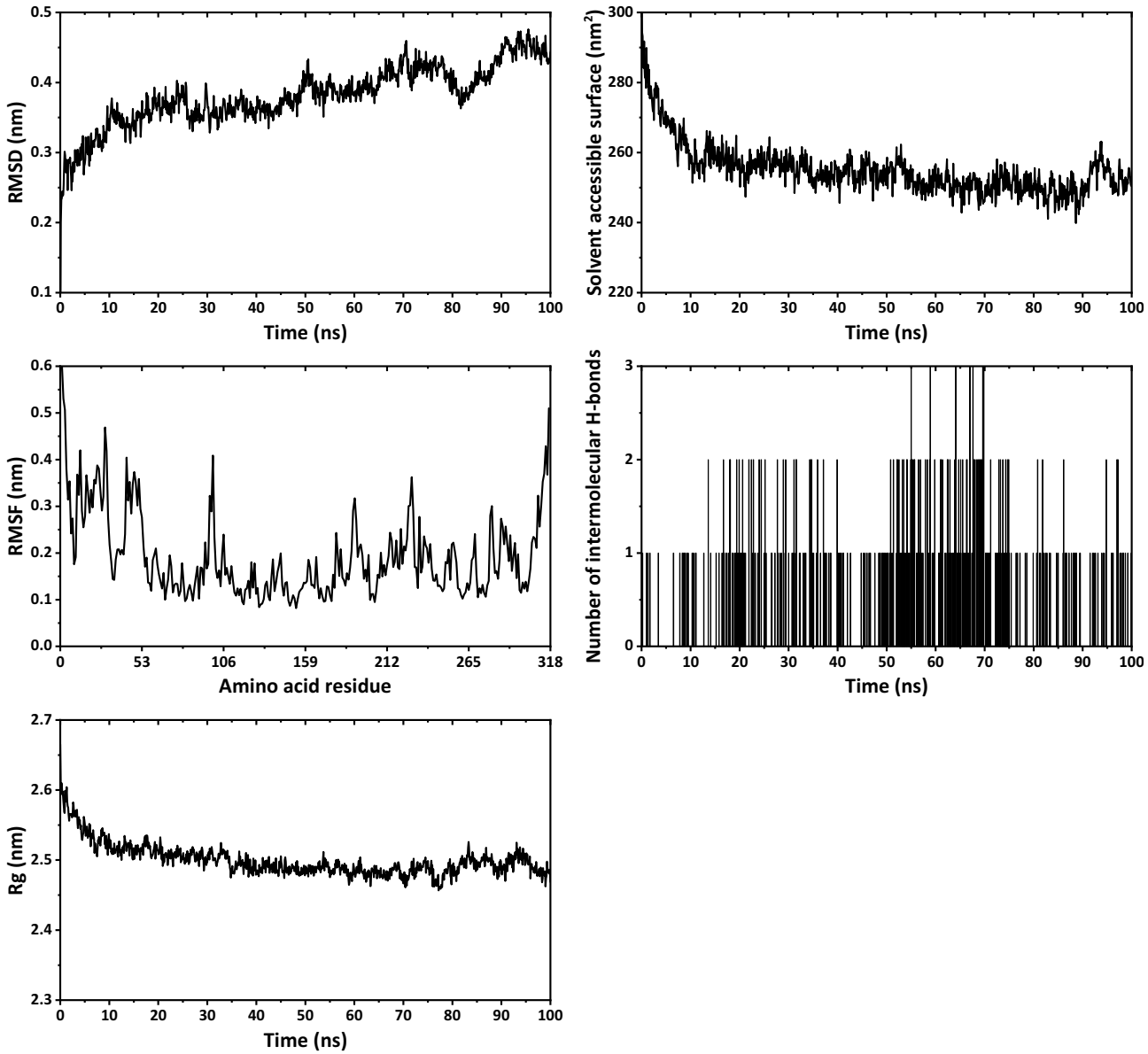

Fig. 9 RMSD, RMSF, Rg, SASA and intermolecular hydrogen bonds analysis profiles of the papain-like protease (PLpro)–betulin complex

Conclusions

We report detailed computational studies of betulin, which is of great interest for its biological properties. The strcuture of betulin was optimized by the DFT/B3LYP/6–311++G(d,p) calculations to verify electronic properties. We have also established values of the global chemical reactivity descriptors, which allowed to reveal electron accepting and donating abilities of the reported compound. Bioavailability, druggability as well as absorption, distribution, metabolism, excretion and toxicity properties of betulin were evaluated using the SwissADME, BOILED-Egg, and ProTox-II tools. As evidenced from the red dot position in the BOILED-Egg plot, both BBB and gastrointestinal absorption properties are negative with the negative PGP effect on the molecule.

Betulin was also found to be of interest as a potential corrosion inhibitor for some important metals used in implants. Electron charge transfer from the molecule of betulin to the surface of all the examined metals (Ti, Fe, Zr, Co, Cu, Cr, Ni, Mn, Mo, Zn, Al, W, Ag, Au) was revealed, of which the best results were obtained for Ni, Au and Co.

In silico molecular docking was applied to probe interactions of betulin with a series of the SARS-CoV-2 proteins as well as one of the monkeypox proteins. It was established that betulin is active against all the applied SARS-CoV-2 and monkeypox proteins with the best binding affinity with papain-like protease (PLpro) and spike protein, RBD (native). The title compound also interacts with spike protein and RBD (mutated), and was also found to be active against the studied monkeypox protein. According to the molecular dynamics simulation data, PLpro forms stable complex with betulin.

Acknowledgements This work was supported by state assignment of the Ministry of Science and Higher Education of the Russian Federation (Project Reg. No. 720000Ф.99.1.Б385АА13000).

Author contribution TMB involved in conducting research, partial analysis of results and preparing a manuscript; MGB and DAS involved in planning research, analysis results and preparing a manuscript; AIK, IAK, LNM, and ANG involved in conducting research and partial analysis of results.

Availability of data and material Not applicable.

Code availability Not applicable.

Declarations

Competing interests The authors declare no competing interests.

References

1. Cragg GM, Grothaus PG, Newman DJ (2014) New horizons for old drugs and drug leads. J Nat Prod 77:703–723
2. Moss GP, Smith PAS, Tavernier D (1995) Glossary of class names of organic compounds and reactivity intermediates based on structure (IUPAC Recommendations). Pure Appl Chem 67:1307–1375
3. IUPAC (1997) Compendium of chemical terminology, 2nd ed. (the "Gold Book"). Compiled by McNaught AD and Wilkinson A. Blackwell Scientific Publications, Oxford. Online version (2019) created by Chalk SJ. ISBN 0–9678550–9–8. https://doi.org/10.1351/goldbook
4. Breitmaier E (2006) Terpenes: flavors, fragrances, pharmaca, pheromones. Wiley-VCH
5. Sami A, Taru M, Salme K, Jari Y-K (2006) Pharmacological properties of the ubiquitous natural product betulin. Eur J Pharm Sci 29:1–13
6. Król SK, Kiełbus M, Rivero-Müller A, Stepulak A (2015) Comprehensive review on betulin as a potent anticancer agent. Biomed Res Int 2015:584189
7. Drąg-Zalesińska M, Borska S (2019) Betulin and its derivatives – precursors of new drugs. World Sci News 127:123–138
8. Lowitz JT (1788) Űber eine neue, fast benzoeartige substanz der briken. Crell's Chem Ann 1:312–317
9. Krasutsky PA (2006) Birch bark research and development. Nat Prod Rep 23:919–942
10. Koptelova EN, Kutakova NA, Tretjakov SI, Faleva AV, Razumov E, Barcík Š (2020) Extraction of betulin from the birch bark balance at pulp and paper production. Wood Res 65:833–842
11. Gotman I (1997) Characteristics of metals used in implants. J Endourol 11:383–389
12. Manivasagam G, Dhinasekaran D, Rajamanickam A (2010) Biomedical implants: corrosion and its prevention - a review, Recent Pat. Corros Sci 2:40–54
13. Aggarwal D, Kumar V, Sharma S (2022) Drug-loaded biomaterials for orthopedic applications: a review. J Control Release 344:113–133
14. Obot IB, Macdonald DD, Gasem ZM (2015) Density functional theory (DFT) as a powerful tool for designing new organic corrosion inhibitors. Part 1: an overview. Corros Sci 99:1–30
15. Goyal M, Kumar S, Bahadur I, Verma C, Ebenso EE (2018) Organic corrosion inhibitors for industrial cleaning of ferrous and nonferrous metals in acidic solutions: a review. J Mol Liq 256:565–573
16. Harvey TJ, Walsh FC, Nahlé AH (2018) A review of inhibitors for the corrosion of transition metals in aqueous acids. J Mol Liq 266:160–175
17. Chauhan DS, Verma C, Quraishi MA (2021) Molecular structural aspects of organic corrosion inhibitors: experimental and computational insights. J Mol Struct 1227:129374
18. Kokalj A (2021) Molecular modeling of organic corrosion inhibitors: calculations, pitfalls, and conceptualization of molecule-surface bonding. Corros Sci 193:109650
19. Ay B, Şahin O, Demir BS, Saygideger Y, López-de-Luzuriaga JM, Mahmoudi G, Safin DA (2020) Antitumor effects of novel nickel–hydrazine complexes in lung cancer cells. New J Chem 44:9064–9072
20. Alkhimova LE, Babashkina MG, Safin DA (2021) α-Aminophosphonates 4-XC_6H_4–NH–CH(4-BrC_6H_4)–P(O)(O^iPr)$_2$ (X = H, Br, MeO): Crystal structures, Hirshfeld surface analysis, computational studies and in silico molecular docking with the SARS-CoV-2 proteins. Tetrahedron 97:132376
21. Shiryaev AA, Goncharenko AN, Burkhanova TM, Alkhimova LE, Babashkina MG, Chandrasekaran R, Safin DA (2021) A chiral (1*R*,2*R*)-*N*, *N*′-bis-(salicylidene)-1,2-diphenyl-1,2-ethanediamine Schiff base dye: synthesis, crystal structure, Hirshfeld surface analysis, computational study, photophysical properties and in silico antifungal activity. J Iran Chem Soc 18:2897–2911
22. Babashkina MG, Frontera A, Kertman AV, Saygideger Y, Murugavel S, Safin DA (2022) Favipiravir: insight into the crystal structure, Hirshfeld surface analysis and computational study. J Iran Chem Soc 19:85–94

23. Alkhimova LE, Babashkina MG, Safin DA (2022) Computational analysis of aspirin. J Mol Struct 1251:131975
24. Alkhimova LE, Burkhanova TM, Babashkina MG, Safin DA (2022) A readily available structural analogue of integrastatins A and B: insight into the crystal structure. Hirshfeld surface analysis and computational study, Tetrahedron 109:132671
25. Sharov AV, Burkhanova TM, Taskın Tok T, Babashkina MG, Safin DA (2022) Computational analysis of molnupiravir. Int J Mol Sci 23:1508
26. Burkhanova TM, Babashkina MG, Taskin-Tok T, Sharov AV, Safin DA (2022) Naphthalene-based bis-*N*-salicylidene aniline dyes: crystal structures, Hirshfeld surface analysis, computational study and molecular docking with the SARS-CoV-2. J Iran Chem Soc 19:1979–1991
27. Alkhimova LE, Sharov AV, Burkhanova TM, Babashkina MG, Safin DA (2022) Ambroxol: insight into the crystal structure, Hirshfeld surface analysis and computational study. Polycycl Aromat Comp. https://doi.org/10.1080/10406638.2022.2049323
28. Babashkina MG, Safin DA (2022) 6-Amino-2-(4-fluorophenyl)-4-(trifluoromethyl)quinoline: insight into the crystal structure, Hirshfeld surface analysis and computational study. Polycycl Aromat Comp. https://doi.org/10.1080/10406638.2022.2068622
29. Babashkina MG, Panova EV, Alkhimova LE, Safin DA (2022) Salen: insight into the crystal structure, Hirshfeld surface analysis, optical properties, DFT, and molecular docking studies. Polycycl Aromat Comp. https://doi.org/10.1080/10406638.2022.2097281
30. Dennington R, Keith TA, Millam JM (2016) GaussView, Version 6.0. Semichem Inc Shawnee Mission KS
31. Frisch MJ, Trucks GW, Schlegel HB, Scuseria GE, Robb MA, Cheeseman JR, Scalmani G, Barone V, Mennucci B, Petersson GA, Nakatsuji H, Caricato M, Li X, Hratchian HP, Izmaylov AF, Bloino J, Zheng G, Sonnenberg JL, Hada M, Ehara M, Toyota K, Fukuda R, Hasegawa J, Ishida M, Nakajima T, Honda Y, Kitao O, Nakai H, Vreven T, Jr Montgomery JA, Peralta JE, Ogliaro F, Bearpark M, Heyd JJ, Brothers E, Kudin KN, Staroverov VN, Keith T, Kobayashi R, Normand J, Raghavachari K, Rendell A, Burant JC, Iyengar SS, Tomasi J, Cossi M, Rega N, Millam JM, Klene M, Knox JE, Cross JB, Bakken V, Adamo C, Jaramillo J, Gomperts R, Stratmann RE, Yazyev O, Austin AJ, Cammi R, Pomelli C, Ochterski JW, Martin RL, Morokuma K, Zakrzewski VG, Voth GA, Salvador P, Dannenberg JJ, Dapprich S, Daniels AD, Farkas O, Foresman JB, Ortiz JV, Cioslowski J, Fox DJ (2013) Gaussian 09. Revision D.01
32. Krishnan R, Binkley JS, Seeger R, Pople JA (1980) Self-consistent molecular orbital methods. XX. A basis set for correlated wave functions. J Chem Phys 72:650–654
33. Becke AD (1993) Density-functional thermochemistry. III. The role of exact exchange. J Chem Phys 98:5648–5652
34. Frisch MJ, Pople JA, Binkley JS (1984) Self-consistent molecular orbital methods 25. Supplementary functions for Gaussian basis sets. J Chem Phys 80:3265–3269
35. O'boyle NM, Tenderholt AL, Langner KM (2008) cclib: a library for package-independent computational chemistry algorithms. J Comput Chem 29:839–845
36. http://gausssum.sourceforge.net/. Accessed 18 June 2022
37. Daina A, Michielin O, Zoete V (2017) SwissADME: a free web tool to evaluate pharmacokinetics, drug-likeness and medicinal chemistry friendliness of small molecules. Sci Rep 7:42717
38. Diana A, Zoete V (2016) A BOILED-Egg to predict gastrointestinal absorption and brain penetration of small molecules. ChemMedChem 11:1117–1121
39. https://tox-new.charite.de/protox_II/index.php?site=home. Accessed 18 June 2022
40. Banerjee P, Eckert AO, Schrey AK, Preissner R (2018) ProTox-II: a webserver for the prediction of toxicity of chemicals. Nucleic Acids Res 46:w257–w263
41. Trott O, Olson AJ (2010) AutoDock Vina: improving the speed and accuracy of docking with a new scoring function, efficient optimization and multithreading. J Comput Chem 31:455–461
42. Eberhardt J, Santos-Martins D, Tillack AF, Forli S (2021) AutoDock Vina 1.2.0: new docking methods, expanded force field, and python bindings. J Chem Inf Modeling 61:3891–3898
43. Rose Y, Duarte JM, Lowe R, Segura J, Bi C, Bhikadiya C, Chen L, Rose AS, Bittrich S, Burley SK, Westbrook JD (2021) RCSB protein data bank: architectural advances towards integrated searching and efficient access to macromolecular structure data from the PDB archive. J Mol Biol 433:166704
44. Systèmes D (2020) BIOVIA Discovery Studio 2020. San Diego: Dassault Systèmes
45. WebGRO for Macromolecular Simulations, https://simlab.uams.edu/. Accessed 10 June 2022
46. Schüttelkopf AW, van Aalten DMF (2004) PRODRG: a tool for high-throughput crystallography of protein-ligand complexes. Acta Crystallogr 60:1355–1363
47. Berendsen HJC, Grigera JR, Straatsma TP (1987) The missing term in effective pair potentials. J Phys Chem 91:6269–6271
48. Groom CR, Bruno IJ, Lightfoot MP, Ward SC (2016) Cambridge Structural Database. Acta Cryst B 72:171–179
49. Pérez P, Domingo LR, Aizman A, Contreras R (2007) Chapter 9 The electrophilicity index in organic chemistry. In: Elsevier BV (ed) Theoretical and Computational Chemistry; A. Toro-Labbé, vol 19. pp 139–291
50. Michaelson HB (1977) The work function of the elements and its periodicity. J Appl Phys 48:4729–4733
51. Shetty P (2020) Schiff bases: an overview of their corrosion inhibition activity in acid media against mild steel. Chem Eng Commun 207:985–1029
52. Kaur M, Kaur K, Kaur H (2021) Quest of schiff bases as corrosion inhibitors: a first principle approach. J Phys Org Chem 34:e4260
53. Verna C, Quraishi MA (2021) Recent progresses in Schiff bases as aqueous phase corrosion inhibitors: design and applications. Coord Chem rev 446:214105
54. Meng X-Y, Zhang H-X, Mezei M, Cui M (2011) Molecular docking: a powerful approach for structure-based drug discovery. Curr Comp Aid Drug 7:146–157
55. Jorgensen WL (2004) The many roles of computation in drug discovery. Science 3030:1813–1818
56. Li H, Wang H-Y, Kang S, Silverman RB, Poulos TL (2016) Electrostatic control of isoform selective inhibitor binding in nitric oxide synthase. Biochemistry 55:3702–3707
57. Tok TT, Tatar G (2017) Structures and functions of coronavirus proteins: molecular modeling of viral nucleoprotein. Int J Virol Infect Dis 2:001–007
58. Tok TT, Gowder SJT (2020) An updated review on Covid-19 with special reference to structural elucidation and functional properties. Biomed J Sci Tech Res 31:24345–24351
59. Shamsi A, Mohammad T, Anwar S, Amani S, Khan MS, Husain FM, Rehman MT, Islam A, Hassan MI (2021) Potential drug targets of SARS-CoV-2: from genomics to therapeutics. Int J Biol Macromol 177:1–9
60. https://www.who.int/emergencies/disease-outbreak-news/item/2022-DON385. Accessed 10 June 2022

Publisher's Note Springer Nature remains neutral with regard to jurisdictional claims in published maps and institutional affiliations.

Springer Nature or its licensor holds exclusive rights to this article under a publishing agreement with the author(s) or other rightsholder(s); author self-archiving of the accepted manuscript version of this article is solely governed by the terms of such publishing agreement and applicable law.